Suspension Polymerization of Acrylamide in an Oscillatory Baffled Reactor: from Drops to Particles

X. Ni and J. C. Johnstone
Dept. of Mechanical Engineering, Heriot-Watt University, Edinburgh EH14 4AS, U.K.

K. C. Symes and B. D. Grey
Ciba Speciality Chemicals, Additives Div., Water Treatments Limited, Bradford BD12 0JZ, U.K.

D. C. Bennett
Dept. of Chemical and Process Engineering, University of Strathclyde, Glasgow G1 1XJ, U.K.

Droplet and particle-size distribution of inverse phase suspension polymerization of acrylamide was studied in an oscillatory baffled reactor (OBR). A discretized population balance model developed estimates the coalescence droplet rate and the type of droplet interactions contributing to the coalescence process in the system. In an OBR, fluid mixing is achieved by eddies generated when a set of prespecified orifice baffles moves periodically through liquid. These vortices can be controlled by a combination of geometrical and operational parameters, such as orifice diameter, baffle spacing, oscillation frequency, and oscillation amplitude. This type of mixing, combining with a close-to-constant level of turbulence intensity in the reactor, has led to a high degree of controllability and repeatability for both droplet and particle size, and a fine particle level significantly lower than a conventional stirred-tank reactor. Generic correlation is established linking the final bead size and Sauter mean droplet size with power dissipation.

Introduction

Generally, there are two types of suspension polymerization processes: the standard suspension polymerization, and the inverse phase suspension polymerization. For the standard suspension polymerization methodology, a water-insoluble monomer is dispersed and suspended in a continuous aqueous phase, usually water, as droplets, and is stabilized by protective colloids or suspending agents. Polymerization is initiated by a monomer-soluble initiator, and polymer particles (beads) occur within the monomer droplets. A number of major polymer products are produced in this way. These include commodity species such as polyvinylchloride and polystyrene, moderate tonnage products such as cation- and anion-exchange resins, and specialities such as high performance liquid chromatography column packings. For the inverse phase polymerization, the name says it all. A water-based monomer phase is dispersed as droplets in a continuous oil phase and polymerized in the droplets to form polymer particles as a dispersed solid phase. During the reaction, the behavior inside each dispersed monomer droplet is that of bulk polymerization (Lin and Wang, 1981). The polymerization process follows a free radical mechanism (Hunkeler and Haimelec, 1991), and is initiated chemically by water soluble free radical azo or peroxide species (Hunkeler, 1992; Hunkeler and Hernandez-Barajas, 1996). The water-soluble polymers are the results. Polyacrylamide is produced by such a process. In fact, the production of water-soluble polymers is part of a multibillion-pound industry. Such polymers are extensively used in processes such as water clarification in the paper making industry and as water treatment coagulants. Though the polymer chemistry involved and the stabilizing systems exploited in both polymerization methodologies are rather different, the basic engineering is common. This involves conventional mechanically agitated stirred-tank vessels

Correspondence concerning this article should be addressed to X. Ni.

operating mainly in batch production. The principal objective in suspension polymerization is the formation of a suspension as uniform as possible of monomer droplets in the continuous phase, and the prevention of coalescence of such droplets during the polymerization process. Efficient mixing within a polymerization vessel serves both purposes. In this work, we report our investigation of inverse phase suspension polymerization of acrylamide beads of required size and specification in a batch oscillatory baffled reactor (OBR) from droplets to final particles. The results and the methods described in this article are applicable to other reactor systems so long as the power dissipation rate is kept the same.

In an OBR, fluid mixing is achieved by eddies that are generated when a set of prespecified orifice baffles moves periodically through liquid. These vortices can be controlled by a combination of geometrical and operational parameters, such as orifice diameter, baffle spacing, oscillation frequency, and oscillation amplitude. Under certain operational conditions, an OBR can be operated as either a plug-flow reactor or an enhanced mixing device (Brunold et al., 1989; Dickens et al., 1989; Mackley and Ni, 1991, 1993). For a given baffle geometry, the fluid mechanical condition in an OBR is controlled by the oscillatory Reynolds number Re_0, and the Strouhal number St defined as

$$Re_o = \frac{Dx_0\omega}{\nu} = \frac{2\pi Dx_0 f}{\nu} = \frac{2\pi Du_{\text{osc}}}{\nu} \tag{1}$$

$$St = \frac{D}{4\pi x_o} \tag{2}$$

where D is the tube diameter (m), x_0 is the center to peak oscillation amplitude (m), ω is the angular frequency of oscillation ($=2\pi f$), f is oscillation frequency (Hz), u_{osc} ($x_0 f$) is the oscillation velocity (m/s), and ν is the kinematic viscosity of the fluid (m^2/s). The power dissipation rate of an OBR can be estimated from (Baird and Stonestreet, 1995) as

$$\epsilon = \frac{P}{\rho V} = \frac{2N_B}{3\pi C_D^2}\frac{1-\alpha^2}{\alpha^2}x_o^3\omega^3 \quad \text{(W/kg)} \tag{3}$$

where N_B is the number of baffles per unit length (/m) relating to the baffle spacing, α is the baffle free area ratio [$=(D_0/D)^2$] accounting for the baffle diameter, where D_0 is the orifice diameter (m), ρ is the density of liquid (kg/m^3), C_D is the orifice discharge coefficient (taken as 0.7). For a given baffle geometry, both the fluid mechanical conditions and the power dissipation rate in an OBR are proportional to the oscillation velocity. In this work, the properties of mean droplet and polymer particle sizes are correlated to the oscillation velocity, and the coalescence rates of droplets are evaluated against the oscillation frequency and amplitude, as well as the oscillation velocity.

Experimental Facilities and Procedure

Oscillatory baffled reactor

The batch OBR system is shown in Figure 1. Unlike the predecessors of OBRs in previous investigations, the oscillatory motion of fluid in this case is achieved by moving a set of periodically spaced baffles up and down the liquid medium at the top of the column, rather than pulsing fluid through a set of stationary baffles at the base. Such an oscillating mechanism has clear advantages in scale-up. The reactor itself consisted of a vertical glass tube of 50 mm in diameter, 1,000 mm in height, and 5 mm in thickness. There were four ports along the reactor: two for monomer charging and nitrogen purging, respectively, and the other two for droplet sampling, as shown in Figure 1. Both sample ports were of 3 mm internal diameter, with one located at the bottom of the reactor and one at the top. A plastic tube of approximately 100 mm long was attached to each sample port. A stainless steel plate was flanged onto the bottom of the glass column and was fitted with a 25 mm diameter valve, allowing the reactor contents to be discharged when required. A set of eight orifice baffles was used in the investigation, and was attached to a coupling plate at the top. The baffles were made of a 3 mm thick stainless steel plate and were connected by two 3 mm diameter stainless steel rods. The baffles were designed to fit closely to the wall of the column. A drive unit, consisting of an electric motor with a flywheel, an inverter, and a linkage cam, provided the periodic motion of the baffles. The speed of the motor controlled oscillation frequencies from 1 to 5 Hz with

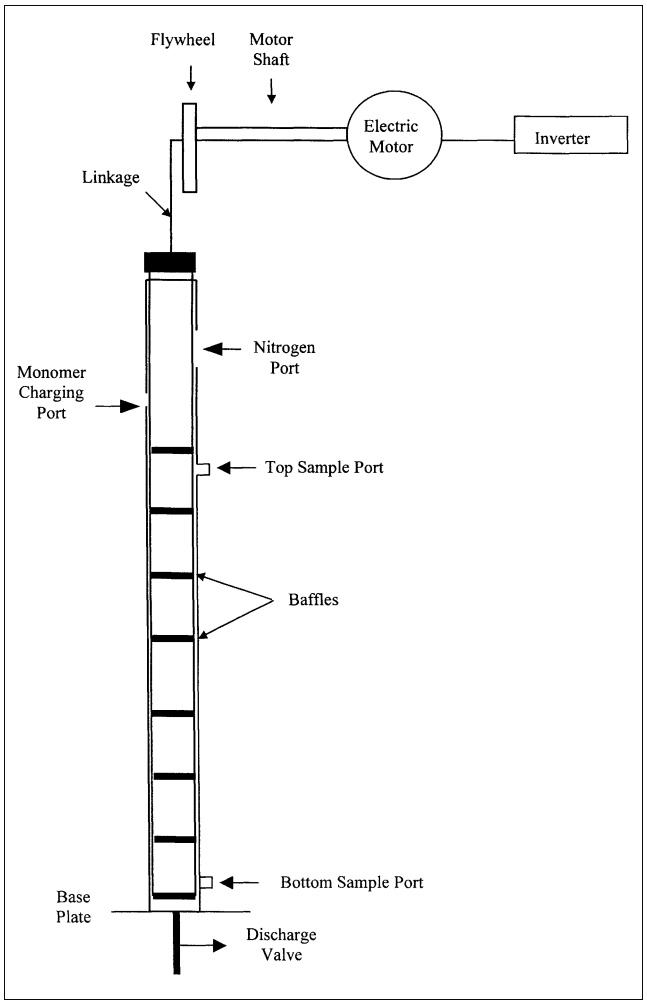

Figure 1. Batch oscillatory baffled reactor.

a 0.01 Hz increment. Oscillation amplitudes of 10 to 50 mm, peak-to-peak, with an increment of 10 mm were obtained by adjusting the eccentric positions of the linkage cam on the flywheel. The free baffle area ratio (defined as the ratio of the orifice area to the tube area) was fixed at 23% and the baffle spacing at 75 mm, which corresponds to 1.5 times the tube diameter.

Monomer

The redox method of initiation was used in the inverse-phase suspension polymerization, that is, the initiators were a redox pair. The two phases in the reaction are an organic phase, which is comprised of iso-paraffinic hydrocarbon (Isopar) with a steric stabilizer, and a monomer phase, primarily of water and acrylamide. Based on a confidential and scaled-down formulation of a proprietary polyacrylamide resin supplied by Ciba Water Treatment Division, U.K. the recipe was specifically formulated to give off much less heat than the traditional ones, that is, maximum reaction temperature is about 50°C. At such a low temperature, the conversion of monomer is still very high in excess of 99%. This recipe allows the performance of inverse-phase suspension polymerization tests without considering the heat-transfer element, as in our case, in a glass OBR with no jacket. The use of the glass vessel also provides good visual observation of what is really happening in the reactor. Although the recipe is proprietary, the methods and procedures described here are common to all inverse-phase suspension polymerization processes utilizing a redox pair as an initiator, and can easily be moved from one reactor to another.

The experimental procedure for each run was as follows: the oil phase, consisting of 750 g Isopar and 3.75 g stabilizer, was prepared and charged into the column. The baffles were then oscillated at a frequency of 1 Hz. Nitrogen sparge was switched on for 30 min at 0.1 bar to degas the oil phase. The monomer phase was prepared using 122.5 g acrylamide, 122.5 g distilled water, 5 g pH buffer, and 0.5 g Sequestrant solution. It was then placed in warm water and stirred occasionally to allow the acrylamide to fully dissolve. In addition, a solution of 20% acetic acid was prepared. Two 50 mL of distilled water were used to prepare both the Redox initiator A and B solutions, respectively.

The 20% acetic acid was added dropwise to the monomer phase until a pH of 6 was achieved and maintained. 2.5 mL of the Redox Initiator A was then added to the monomer phase under oscillation, and the resulting mixture was immediately charged to the OBR. The reactants were left for 3 min in order for oxygen in the monomer phase to fully disperse into the oil phase. After the 3 min 2.5 mL of the Redox initiator B was added to the OBR to initiate the reaction. Then, 30 min later, the contents of the reactor were collected and the beads were dehydrated. Samples of dried polymer particles were sent to the Ciba Water Treatment Division for analyses, where the particle-size distributions were measured using a Sympatex machine (which utilizes a light scattering technique), and the molecular-weight distributions were measured by the intrinsic viscosity method.

For droplet experiments, both the Redox initiators A and B were not employed. Furthermore, 2.6 g of para-methoxy phenol, an inhibitor, was dissolved in the monomer phase in order to prevent the polymerization reaction from taking place during the experiments. Droplet samples were taken at the end of the 3 min mixing time from either the top or bottom of the reactor.

Sampling method

Due to the nature of the recipe used in the investigation, droplets did coalesce when fluid oscillation was either reduced or removed, so the sampling method proved to be critical. After extensive tests, a reliable sampling method was developed: a sample of approximately 5 mL was released from a sample port into a 50 mL beaker containing a 20 mL solution of 80% Isopar and a 20% stabilizer. It was important to submerge the plastic sampling tube under the surface of the solution so those droplets are immediately surrounded by the stabilizer solution, preventing coalescence from occurring. A disposable pipette was then used to place six separate sample drops, each approximately 50 μL apart on two microscope slides, with three drops each. The slides were examined under a microscope at 40 times magnification.

Image capture and droplet analysis

The image capture unit is shown in Figure 2. The system consisted of a charged coupled device (CCD) camera mounted on top of a microscope, a computer video capture card, and a PC. The CCD camera took four digital pictures of each of the six sample drops, that is, 24 pictures containing approximately 500 droplets per experiment. These photographs were then treated, applying the photographic software package Paintshop Pro 6 before they were analyzed using the Aequitas image analysis software to determine the droplet-size distribution. The pretreatment included the edge, brightness, and contrast enhancement. The Aequitas software measured the inside diameter of the droplets, and this may increase calculation errors when the edge thickness of the droplets was different for varying for varying focal lengths (refer to Figure 3). We found that the outside diameter was 1.2 times the inside diameter and this factor has been applied to all droplet analysis. The results produced by the Aequitas software were manipulating using Microsoft Excel to produce the droplet-size distribution (DSD) graphs. From such distri-

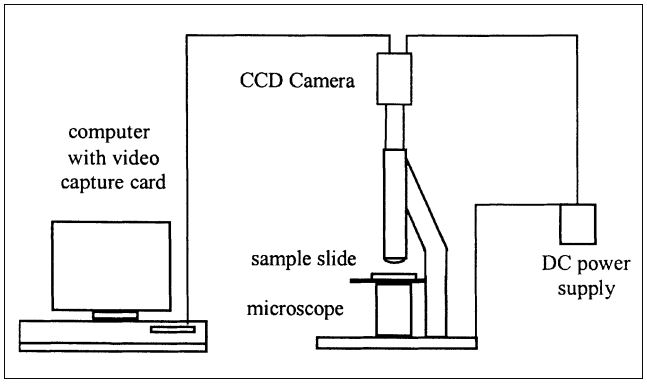

Figure 2. Image analysis unit.

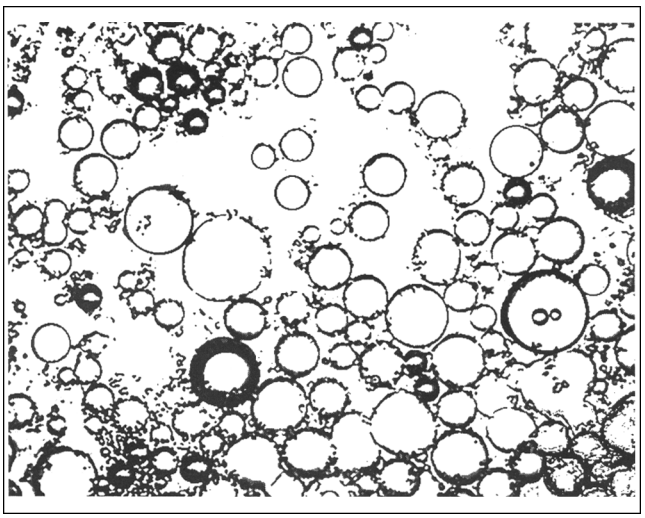

Figure 3. Typical droplet image.

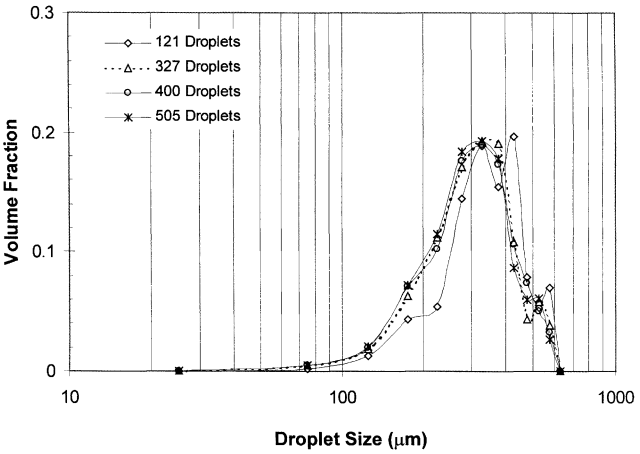

Figure 4. Effect of droplet number on droplet-size distribution.

Oscillation velocity = 80 mm/s, oscillation frequency = 2 Hz; oscillation amplitude = 40 mm; baffle spacing = 75 mm and baffle free area = 23%.

butions, the mean droplet size can be calculated via

$$d_{32} = \frac{\Sigma n_i d_i^3}{\Sigma n_i d_i^2} \qquad (\mu\text{m}) \tag{4}$$

where d_{32} is the Sauter mean droplet size, and n and d are the droplet number and diameter, respectively.

Droplet number

Since droplet analysis is time-consuming, it is essential to identify the minimum number of droplets required to obtain a true reflection of the dispersion within the column. Four different quantities of droplets ranging from 121 to 505 were investigated, and graphs of the DSD were produced and shown in Figure 4. The volume fraction in the vertical axis is defined as

$$\text{Volume Fraction} = \frac{n_i d_i^3}{\Sigma n_i d_i^3} \tag{5}$$

It can be seen that the DSDs are essentially of a Gaussian function and the difference in such distributions between 327 and 505 droplets was minimal. As a result, it was felt that 400 droplets would be sufficient for all the experiments.

Uniformity

The uniformity of the droplets was examined by taking samples from two different locations along the column and at different mixing times. The oscillation velocity used for all the experiments was 90 mm/s. Droplets were sampled at both the top and bottom ports at a fixed mixing time of 3 min, and further samples were taken from the bottom port only at mixing times of 6 and 10 min. The results are shown in Figure 5. It was clear that, after a mixing time of 3 min, the top and bottom samples were almost identical. This suggests that a stable and uniform suspension had been formed throughout the reactor at that time, and a droplet sample from either port is truly representative of the suspension. Increased mixing times of 6 and 10 min had an insignificant effect on the DSD at the bottom of the reactor, indicating that once the uniformity was reached in the OBR, it remained independent of the mixing time.

Repeatability

The repeatability tests were carried out at identical operating conditions, but on three different days. The results can be seen in Figure 6. It is clear that a high degree of repeatability was obtained with all the DSD profiles.

Results and Discussion

Before presenting results, it should be pointed out that the makeups of the recipe have been kept unchanged throughout

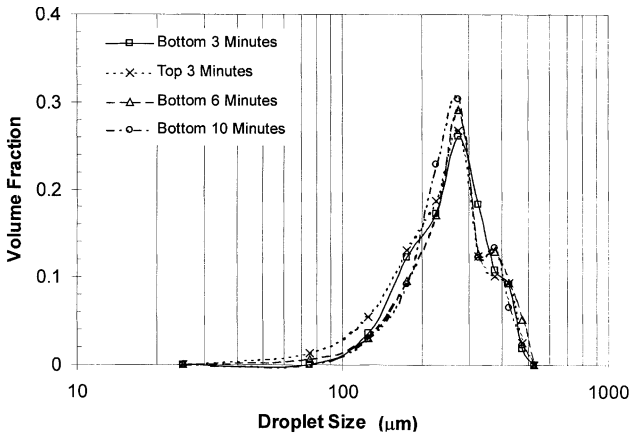

Figure 5. Effect of mixing time on droplet-size distribution.

Oscillation velocity = 90 mm/s; oscillation frequency = 2.25 Hz; oscillation amplitude = 40 mm; baffle spacing = 75 mm and baffle free area = 23%.

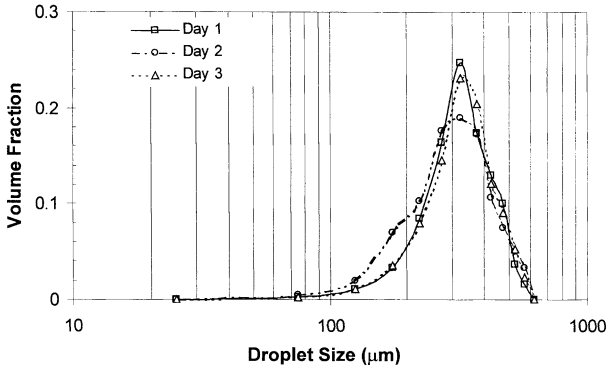

Figure 6. Repeatability of droplet-size distribution.

Oscillation velocity = 80 mm/s; oscillation frequency = 2 Hz; oscillation amplitude = 40 mm, baffle spacing = 75 mm and baffle area = 23%.

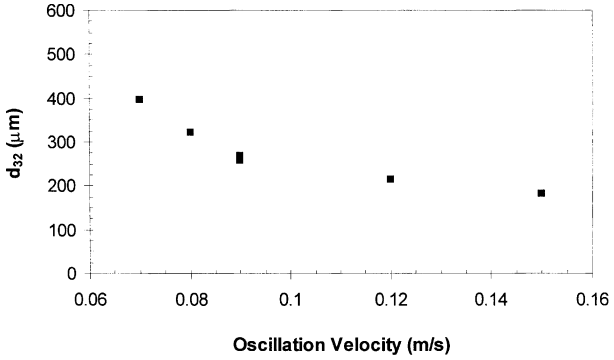

Figure 8. Effect of oscillation velocity on the Sauter mean diameter.

Baffle spacing = 75 mm and baffle free area = 23%.

the study. In this way, the effect of fluid mechanical factors on droplets/particles can be fully investigated. Varying concentrations of the constitutive materials in the recipe commonly leads to unpredictable step changes in drop and particle sizes, and such studies are out of the scope of this work.

Mean droplet size

Figures 7 and 8 show the effect of the oscillation velocity on the droplet-size distribution and on the Sauter mean droplet size, respectively. It is evident that an increase in the oscillation velocity shifted the DSD from right to left and narrowed the distribution of droplets (Figure 7). It also decreased the mean droplet size (Figure 8). This is expected, since the oscillation velocity governs the power input to the system; hence, an increase in the oscillation velocity increased the mixing intensity. Based on the experiments carried out, the following correlation was obtained

$$d_{32} = 2.8 \times 10^{-5} (x_0 f)^{-0.96} \quad \text{(m)} \tag{6}$$

The individual effect of either the oscillation amplitude or frequency on the Sauter mean droplet size was investigated by holding one of the two parameters unchanged while varying the other. The effect of the oscillation amplitude on d_{32} was examined at a constant frequency of 3 Hz, and the effect of the oscillation frequency at a fixed amplitude of 40 mm. The results are shown in Figures 9 and 10, plotted on a log-log scale. An increase in either the oscillation amplitude or frequency decreased the Sauter mean droplet size, with gradients of -0.76 and -1.12 respectively. This suggests that the oscillation frequency had a more prominent effect on d_{32} than the oscillation amplitude. This finding is different to the previous work in the OBR (Ni et al., 1999) where the fluid oscillation was achieved by pulsing fluid at the base of the reactor, as well as the work in a reciprocating plate column (RPC) (Baird and Lane, 1973). In the above two cases, the effect of oscillation frequency on d_{32} was more or less equal to that of oscillation amplitude. The reason for this discrepancy could probably be attributed to the different design of the reactors. When the fluid oscillation in an OBR is achieved by means of oscillating baffles at the top of the reactor, the amplitude in question is usually larger than that, by means of pulsing fluid at the base. The mixing in this case is more sensitive to the change of oscillation frequency. Although there is similarity in the oscillating mechanism between our system and the RPC, the multiperforated plates in the RPC somehow reduce such frequency sensitivity.

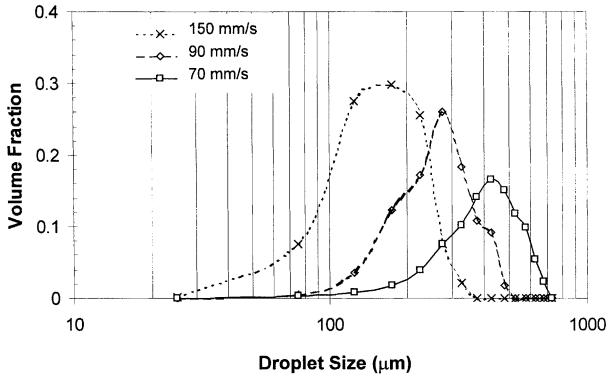

Figure 7. Effect of oscillation velocity on droplet-size distribution.

Baffle spacing = 75 mm and baffle free area = 23%.

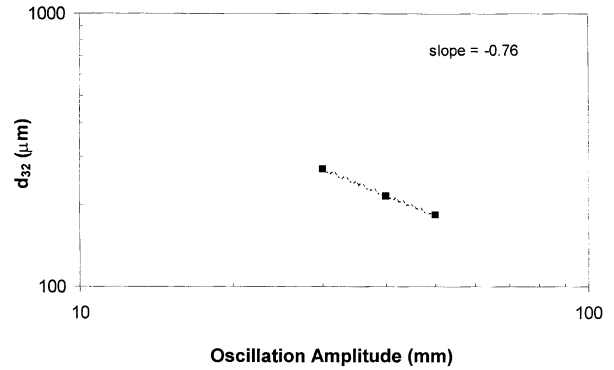

Figure 9. Effect of oscillation amplitude on Sauter mean diameter.

Oscillation frequency = 3 Hz; baffle spacing = 75 mm and baffle free area = 23%.

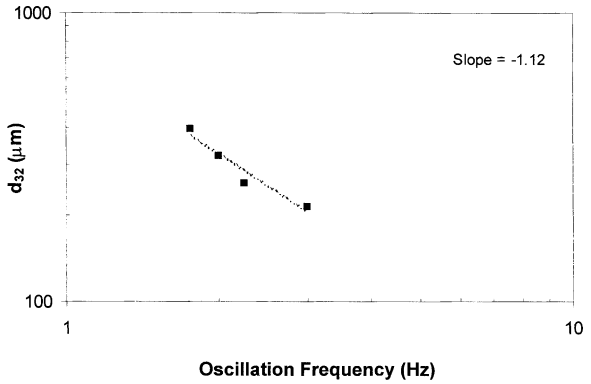

Figure 10. Effect of oscillation frequency on Sauter mean diameter.

Oscillation amplitude = 40 mm; baffle spacing = 75 mm and baffle free area = 23%.

A more generic correlation adopted by all other reactor systems is to relate the Sauter mean droplet size (d_{32}) with the power dissipation ϵ in the given system as

$$d_{32} = 7.26\times10^{-4}\epsilon^{-0.32} \quad \text{(m)} \qquad 10 < \epsilon < 90 \ \text{(W/kg)} \quad (7)$$

The power index of -0.32 was of a similar magnitude to that of -0.4 observed by Ni et al. (1999) in the standard suspension polymerization of methylmethacrylate in an OBR of the same diameter. This suggests that the two OBR systems are similar in the mechanism of droplet formation, and the Kolmogoroff's isotropic turbulence is present in both reactors.

Table 1 compares the K values (where $K = d_{32}/\epsilon^{-0.4}$) for different devices, and, for our system, $\sigma = 2\times10^{-4}$ N/m and $\rho = 825$ kg/m^3. The K value is essentially a parameter that describes the characteristics of a given liquid-liquid dispersion and provides a useful comparison with more conventional reactor systems. It can be seen that the K values calculated for RPCs are generally lower than for the other systems due to the number of perforations present in each plate, that is, the energy dissipation per hole will be less than that in an OBR. The K values quoted range from 2.26×10^{-4} to 9.72×10^{-4}, and the value determined for the OBR falls within this range, indicating that the liquid-liquid dispersion characteristics in the OBR are similar to those in the conventional systems. Consequently, the methods and results reported in this article are applicable to other conventional systems.

Coalescence rate of droplets

Due to the nature of the recipe used and the presence of stabilizers within the system, there is little droplet breakage observed after the typical mixing time of 3 min. However, there is apparent droplet coalescence taking place when the mixing intensity is reduced. The droplet data obtained can therefore be used together with a discretized population balance equation to estimate the rate of coalescence of droplets. As described earlier, the droplet samples were taken after 3 min of mixing at which a stable droplet distribution has been achieved. Under such conditions, the volume fraction of droplets is no longer a function of time, but changes with operational parameters. Consequently, droplet data of varying oscillation amplitude, frequency, and velocity can be used to estimate the change in the rate of droplet coalescence against these parameters.

Table 1. Comparison of K Values for Different Devices

Equipment and References	$K\times10^4$
RPC (Baird and Lane, 1973)	3.83
RPC (Boyadzhiev and Spassov, 1982)	2.26
STR (Zerfa and Brooks, 1996)	2.57
STR (Coulaloglou and Tavlarides, 1976)	9.72
OBR (this work)	7.26

Droplet interactions are generally modeled using either Monte Carlo techniques or the population balance equation (PBE), although other methods have also been considered (Zeitlin and Tavlarides, 1972; Narsimhan et al., 1979; Muralidhar and Ramkrishna, 1986; Das et al., 1987; Muralidhar et al., 1988). The Monte Carlo techniques, although both powerful and flexible, are not practical in many situations due to the large computational time required. The PBE has received increasing attention since the early development by Valentas and Amundson (1966) and Valentas et al. (1996), and Coulaloglou and Tavlarides (1977). Laso et al. (1987) proposed a simplification to the PBE, reducing the computational difficulties involved in the numerical solution. The assumption of breakage being a first-order (binary) process, and coalescence being a second-order (equally sized droplets only) process, and the application of a geometrical discretization of droplet volume with a step of $2^{1/2}$ allow faster and simpler solutions than the full PBE. Hounslow et al. (1988) applied the discretized form of the PBE to batch systems, which was also extended to continuous systems (Hounslow, 1990). More recently, Litster et al. (1995) extended this further to incorporate an adjustable discretization. In this work we adopted the discretized PBE to determine the coalescence rate in the system.

Model Development and Coalescence Rate. Experimental droplet data in terms of volume fraction were used in the model. Droplet diameters were discretized into volume bins using the method of Litster et al. (1995) with a minimum droplet diameter of 2 μm and geometric step of $2^{1/6}$ (corresponding to a volume ratio of $2^{1/2}$, illustrated by Figure 11) in all 51 droplet size ranges presented in the distributions. Data for oscillation amplitudes of 30, 40, and 50 mm, oscillation frequencies of 1.75, 2, 2.25 and 3 Hz and oscillation velocities of 70, 80, and 90 mm/s were interpolated into the discretized volume bins assuming a constant droplet size density number

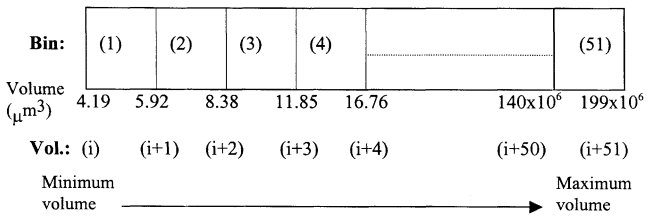

Figure 11. Discretized volume bins used in the population balance equation.

for each of the measured droplet-size ranges. This assumption may be inadequate, but with noisy measured droplet-size distributions, higher order interpolations may introduce further errors.

In establishing the model we also assume that a droplet in a given bin (i) can coalesce with: (a) a drop in the same bin—Type (a); (b) a drop in a bin immediately below or above (i), that is, bins ($i \pm 1$)—Type (b); (c) a drop in a bin immediately below bin ($i \pm 1$), that is, bins ($i \pm 2$)—Type (c).

The resulting droplet volume will be equal to the sum of the two coalescing droplets and, due to the discretization applied, will always move into a bin of a larger droplet volume. Clearly, the more possibilities of droplet interactions to be included, the fuller the coalescence investigation; however, this leads to more complex model equations and requires longer computational time. On balance, our simplified cases would allow us to compute a representative coalescence rate in a reasonable time scale.

The constitutive equations are as follows. Let us denote d_i^*, $F_i(x)$ and $\beta_{i,j}$ as the geometric mean diameter, droplet volume fraction and coalescence rate of droplets in bin (i) with bin (j), with $i = 1$ corresponding to the smallest droplet range and $i = 51$ to the largest. The rate of droplet volume fraction changing with oscillation frequency, amplitude, or velocity is associated with the following six terms as

$$\frac{dF_i}{d\eta} = -F_i(2\beta_{i,i} + \beta_{i,i-1} + \beta_{i,i+1} + \beta_{i,i-2} + \beta_{i,i+2}) + 2\beta_{i-2,i-2}F_{i-2} + K_1\beta_{i-2,i-3}(F_{i-2} + F_{i-3}) + K_2\beta_{i-2,i-1}(F_{i-2} + F_{i-1}) + K_3\beta_{i-2,i-4}(F_{i-2} + F_{i-4}) + K_4\beta_{i-3,i-1}(F_{i-3} + F_{i-1}) \quad (8)$$

where η is a characteristic parameter, and could be the oscillation frequency, amplitude, or oscillation velocity, giving the corresponding unit of the coalescence rate per Hz, per mm or per mm/s, and K1 − K4 are the fraction of the resulting droplets that move to bin (i). The first term on the right accounts for the loss of droplets from bin (i) due to coalescence of the Type (a), (b) or (c), as detailed previously. The second term reflects the gain of droplets in bin (i) by coalescence of the Type (a) from bin ($i-2$). The third and fourth terms are responsible for the gain of droplets in bin (i) by coalescence of the Type (b) from bins ($i-2$) and ($i-3$) or ($i-2$) and ($i-1$), respectively. The remaining terms reflect the gain of droplets in bin (i) by coalescence of the Type (c) from bins ($i-2$) and ($i-4$) or ($i-3$) and ($i-1$), respectively. The predicted droplet volume fraction is then given by

$$F_i^*(\eta_2:\eta_1) = F_i(\eta_1) + \int_{\eta_1}^{\eta_2}\left(\frac{dF_i}{d\eta}\right)d\eta \quad (9)$$

The coalescence rate $\beta_{i,j}$ was estimated from the experimental droplet data by finding values for the coalescence rates that minimize the function

$$\sum_{j=1}^{y-1}\sum_{k=j+1}^{y}\left\|\left[F_i^*(\eta_k:\eta_j) - F_i(\eta_k)\right]\right\|^2 \quad (10)$$

where y is the number of datasets used.

The integration in Eq. 9 is carried out with either an oscillation amplitude step of 10 mm, an oscillation frequency step of 0.25 Hz, or an oscillation velocity step of 10 mm/s using Euler's method. A solution to Eq. 10 can be obtained using the MatLab *fminsearch* function. The computational time required to complete 10,000 iterations of the minimization varied from 3 min when using three datasets, to 12 min when using six datasets. A final solution was usually reached after between 5 and 8 of these cycles, that is, the total computational time varied between 15 and 96 min.

The overall coalescence rate for droplets in a given bin is the sum of all possible combinations of droplet coalescence listed in the assumptions

$$\beta_{\text{Total},i} = 2\beta_{i,i} + \beta_{i,i-1} + \beta_{i,i+1} + \beta_{i,i-2} + \beta_{i,i+2} \quad (11)$$

Figures 12–14 show the calculated overall coalescence rates for each of the operational parameters studied. It should be noted that the range of droplet diameters included in these figures (200 to 600 μm) is larger than that shown in Figures 8–10 of 200 to 400 μm for d_{32}. However, this is expected, as the small fraction of droplets diameter larger than 400 μm that existed in the experimental data can result in artificially high or low predicted rates for these volume bins, as shown in Figures 12–14. As a consequence of this, the calculated coalescence rates in the range of 200 to 400 μm should be closely looked at.

The effect of reducing the oscillation amplitude on the overall coalescence rate is shown in Figure 12. A general decreasing trend in the overall coalescence rate with increasing droplet diameter can clearly be seen. Figure 13 shows the effect of decreasing the oscillation frequency on the calculated overall coalescence rate. The rate in this case generally increases at first, then decreases in the droplet diameter range 200 to 400 μm, and the trend repeats for droplets above 400

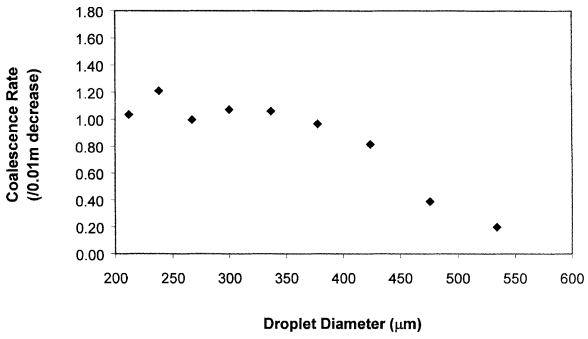

Figure 12. Predicted overall coalescence rate in the droplet diameter range of 200—600 μm for each 10 mm decrease in oscillation amplitude.

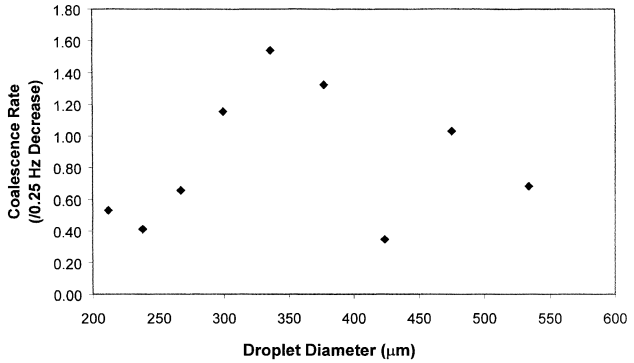

Figure 13. Predicted overall coalescence rate in the droplet diameter range of 200—600 μm for each 0.25 Hz decrease in oscillation frequency.

μm. The different trend and higher coalescence rates in comparison to those for changes in the oscillation amplitude suggests that the coalescence process is more sensitive to changes in the oscillation frequency in the system. This is consistent with our earlier discussion on the mean droplet size.

The variation in the overall coalescence rate for each 10 mm/s decrease in the oscillation velocity is shown in Figure 14. For droplet diameters of 200 to 400 μm, the coalescence rate is more or less the same, with an acceptable level of scattering. The trend is, however, considerably different for extremely large droplet sizes (> 400 μm) where the rate increases with the droplet diameter. This can again be attributed to the small fraction of droplets found in these ranges, resulting in artificially high coalescence rates. Although the individual effect of decreasing either the oscillation frequency or amplitude on the rate differs, the collective effect on the rate is rather small. In the droplet range of 200 to 400 μm, the predicted overall mean coalescence rate is around about 0.35 per 10 mm/s decreasing in the oscillation velocity. As all the droplet measurements were made after 3 min of mixing time, a stable droplet distribution has already been achieved. The ability to take *in-situ* measurements of droplets during the 3 min will allow a further picture of coalescence to emerge. However, this is limited by the practicality, that is, the time taken for sampling.

Since the coalescence rates for each type are automatically calculated in the minimization process, this provides us with a tool to examine which type of droplet interaction contributes more to the coalescence process in the system. The individual rates are as follows

$$\beta_{\text{Type}(a)i} = 2\beta_{i,i} \tag{12}$$

$$\beta_{\text{Type}(b)i} = \beta_{i,i-1} + \beta_{i,i+1} \tag{13}$$

$$\beta_{\text{Type}(c)i} = \beta_{i,i-2} + \beta_{i,i+2} \tag{14}$$

Figures 15–17 show the calculated coalescence rates for each type of coalescence considered, with the operational conditions corresponding to these in Figures 12–14. It can be seen that the coalescence Type (b) clearly has a dominating influence on the droplet formation in the range of 200 to 400 μm (ignoring the extremely high droplet diameters) in all these figures. This rather interesting finding gives measure of the pattern of droplet interactions in the coalescence process of the given system. Such positive identifications pave the way for the more detailed mathematical modeling of coalescence mechanism. As to why drops of different but similar size coalesce, the reason is unclear at the moment. The question of how to utilize such drop interactions to control coalescence and subsequent drop formation will remain a great challenging task for us all. If such controls were feasible, desired drop sizes could be selected in any given reactor system, which can only be a fantasy at the current stage.

It is important to point out that the model presented here can be adopted by other traditional reactor systems as long as droplet-size distributions are measurable.

It should be noted that there are some unphysical (negative) predicted values for the coalescence rate (Figures 15—17), in particular in the case of decreasing frequency. This could probably be due to the fact that the sets of droplet-size distributions used in the modeling shifted to the right with the decrease of the oscillation frequency, while the peak of the volume fraction for the sets did not correspond faithfully, resulting in some negative values for individual co-

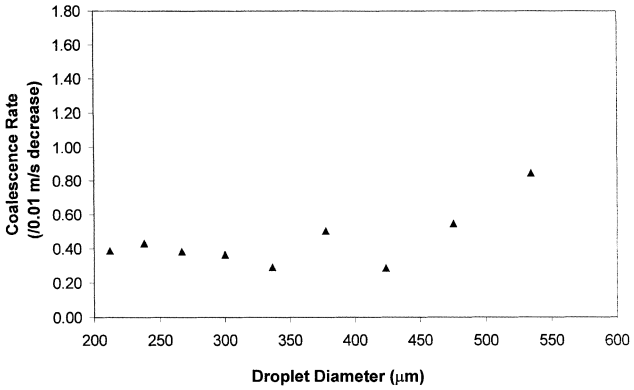

Figure 14. Predicted overall coalescence rate in the droplet diameter range of 200—600 μm for each 10 mm/s decrease in oscillation velocity.

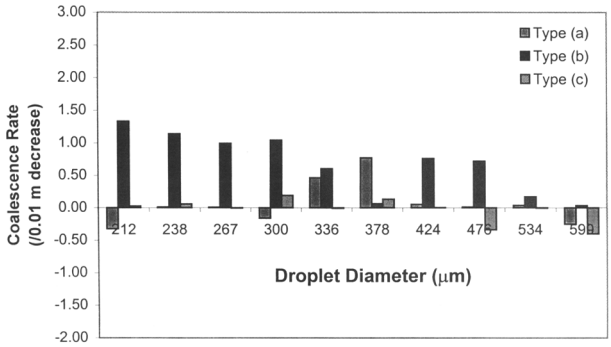

Figure 15. Predicted individual coalescence rates in the droplet diameter range of 200—600 μm for each 10 mm decrease in oscillation amplitude.

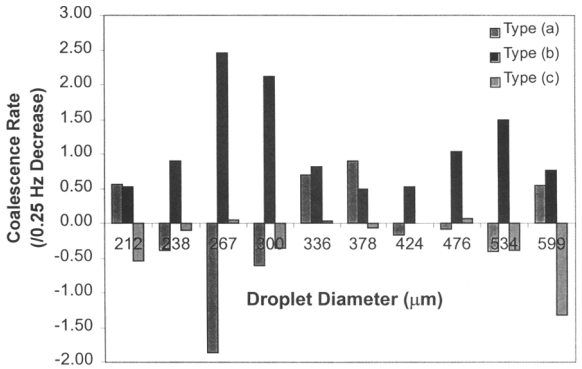

Figure 16. Predicted individual coalescence rates in the droplet diameter range of 200—600 μm for each 0.25 Hz decrease in oscillation frequency.

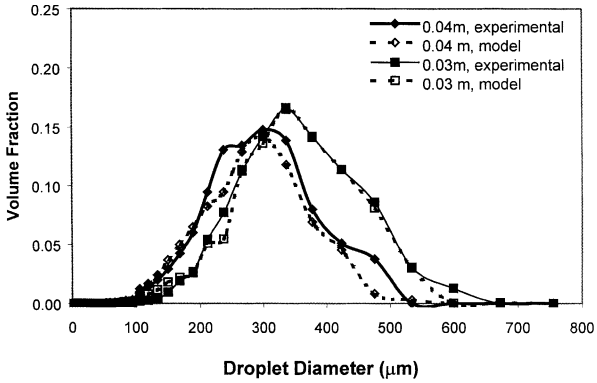

Figure 18. Comparison of reconstructed DSDs with experimental DSDs for varying oscillation amplitude.

alescence rates in the modeling process. In this respect, those negative values should be ignored.

Model Evaluation. Substituting the calculated coalescence rate into Eq. 9, we can reconstruct the droplet-size distributions for every given operational condition, and these can then be compared with experimentally measured DSDs. In such a way, our model can be validated and assumptions justified. Figures 18–20 show such comparisons for changing oscillation amplitude, frequency, and oscillation velocity, respectively. It can be seen that the DSDs predicted by the model match the experimental data closely for all the conditions under a test, and the deviation of the model predictions from the experimental data estimated using the sum of squares method was very small, ranging from 0.01% to 8.71%, thus confirming that the model developed describes the overall and individual coalescence rates in the system with a high degree of accuracy. The model also provides insight into the understanding of the mechanism of droplet formation. It may also prove to be a useful tool in evaluating droplet-size distributions under changing conditions of oscillation.

Mean particle size

Particle-size distribution (PSD) was measured using a Sympatex machine for all the polymerization experiments, and it can be seen that there were very few fines produced (beads with a particle size less then 150 μm), the level of which was consistently less than 3% for all the experimental runs. It can be seen that the PSD was essentially of a Gaussian distribution, and Figure 21 shows merely one out of 100 experiments carried out at a wide range of oscillation conditions. It should be noted that 15% of the total 100 experiments were repeated for the purpose of repeatability, and the closeness of the PSD curves under test gave an indication of the high degree of reproducibility. From the distribution data, the mean particle size of polymer can be determined. The commonly used term for this is the particle size at 50% cumulative volume, that is, $d_{\upsilon,0.5}$. Figure 22 shows the effect of the oscillation velocity on the mean particle size. Similar to the droplet case, an increase in the oscillation velocity decreased the mean particle size and the trend was more pronounced at lower oscillation velocities. Significantly, a Gaussian distribution has remained in the PSDs for all the oscillation velocities. The results shown in Figure 22 are very important as they indicate that the mean particle size and size distribution

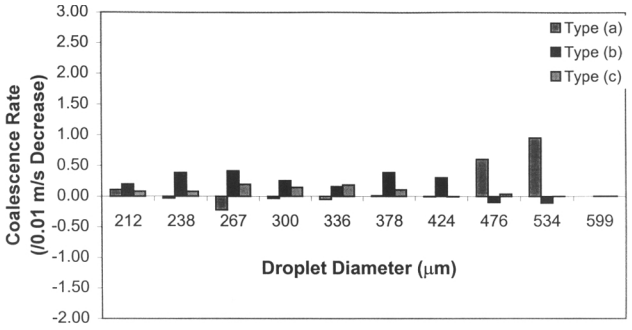

Figure 17. Predicted individual coalescence rates in the droplet diameter range of 200—600 μm for each 10 mm/s decrease in oscillation velocity.

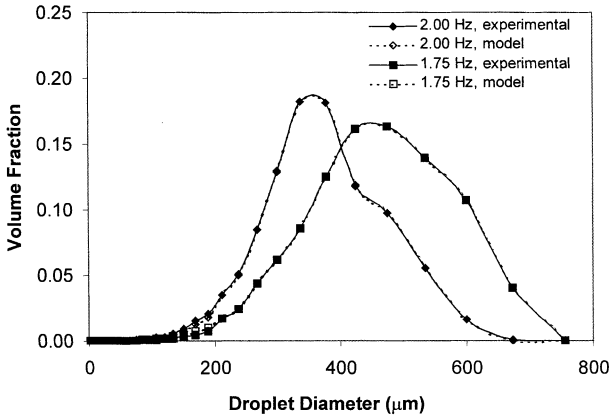

Figure 19. Comparison of reconstructed droplet-size distributions with experimental distributions for varying oscillation frequency.

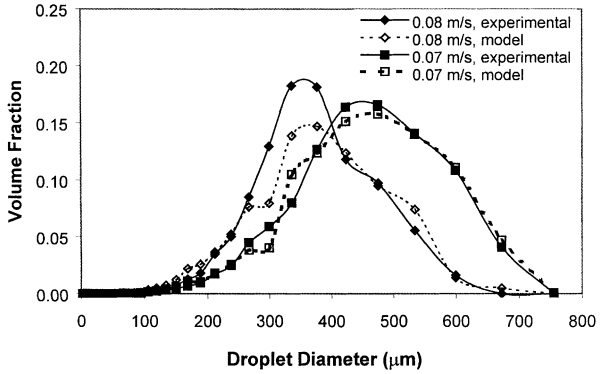

Figure 20. Comparison of reconstructed droplet-size distributions with experimental distributions for varying oscillation velocity.

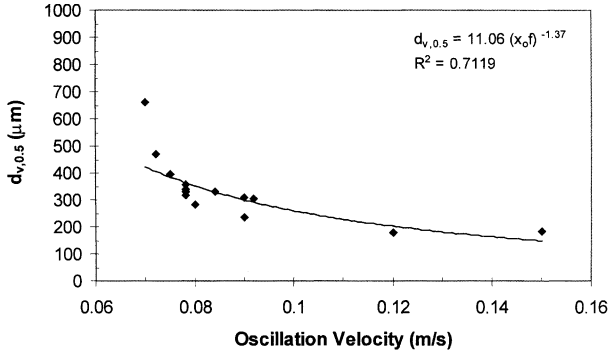

Figure 22. Effect of oscillation velocity on mean particle size.

Baffle spacing = 75 mm and baffle free area = 23%.

in the OBR can be controlled simply by selecting the appropriate oscillation velocity. The range of the mean particle size achieved while maintaining the Gaussian size distribution in the OBR is a key for product engineering.

Based on experimental data, a universal correlation linking $d_{v,0.5}$ with the power dissipation of the system was obtained

$$d_{v,0.5} = 1.44 \times 10^{-3} \epsilon^{-0.55} \quad \text{(m)} \tag{15}$$

This generic correlation can be used as a good guide if the methods are applied to other conventional systems. One of our particular aims in this work was to establish a correlation between the size of the polymer beads produced and that of the droplets. By rearranging Eqs. 7 and 15 the following correlation was obtained

$$d_{v,0.5} = 34.85(d_{32})^{1.70} \quad \text{(m)} \tag{16}$$

By plotting both $d_{v,0.5}$ and d_{32} against the oscillation velocity $x_o f$ in Figure 23, it is clear that the sizes of the droplets and the final beads are close to each other for the entire range of the oscillation velocities examined (70 to 150 mm/s). This is consistent with the small coalescence rates of droplets predicted by the model, which further validates the reliability of the model development. It is also possible to apply Eq. 16 to predict the final mean particle size in the OBR from the droplet size measured prior to the reaction. This exercise can also be adopted by other traditional reactor systems in inverse-phase suspension polymerization.

We have also carried out the evaluation of polymer beads produced from a STR and an OBR. To do so, six experiments were performed at Ciba in a STR using the identical recipe to that in this work, but only 40% of the OBR load, due to the smaller internal volume of the Ciba vessels. All the experiments performed at Ciba used the optimum impeller speed and the mean particle sizes obtained were from 200 to 250 μm. It was possible to produce larger beads in the STR, but at a cost of an increased risk of agglomeration. The OBR has not only produced beads that matched this specification in terms of the mean particle size and distribution width, but also, importantly, manufactured polymer beads that have the mean size ranging from 200 up to 800 μm, while still maintaining a Gaussian particle-size distribution throughout. Furthermore, the OBR has the ability to pro-

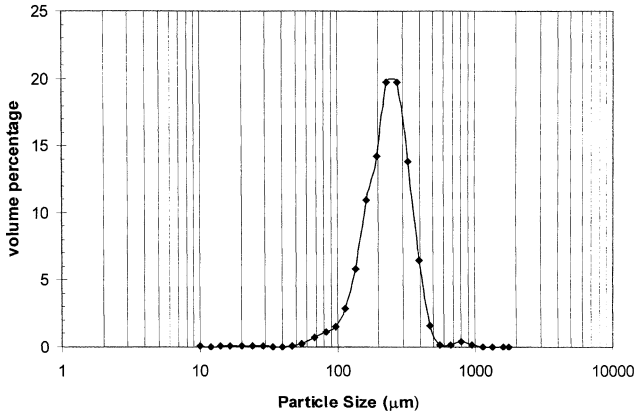

Figure 21. Particle-size distribution: $d_{v,0.1} = 138.3$ μm, $d_{v,0.5} = 234.6$ μm and $d_{v,0.9} = 355.3$ μm.

Oscillation amplitude = 40 mm; oscillation frequency = 2.25 Hz, baffle free area = 23%; baffle spacing = 75 mm and monomer addition time = 20 s.

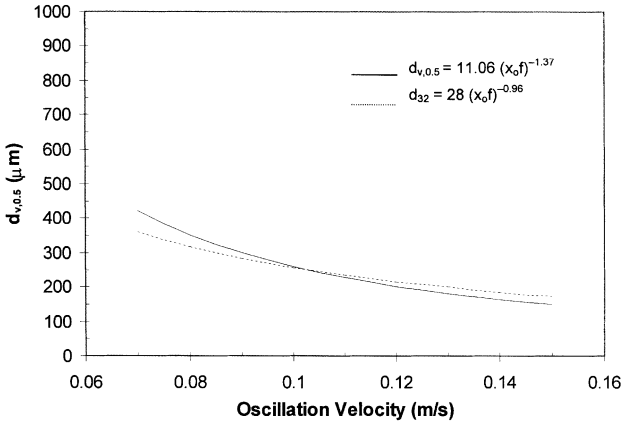

Figure 23. Comparison of mean particle- and droplet-size correlations.

duce polymer particles with a constant level of fines of approximately 3%, which is not obtainable in a STR of a typically 8.5%. A low level of fines in the product is desirable, as it improves the product properties and reduces waste.

Conclusions

We have demonstrated that the OBR is capable of controlling the formation of droplets and, thereafter, producing beads of required specification by simply selecting appropriate operational parameters. Our extensive experimental studies of droplet-size distribution have led to a successful modeling of the coalescence of droplets in the system. The modeling process has also provided the detailed insight of the type of droplet interactions contributing to coalescence process in the system, assisting our understanding on the mechanism of droplet formation. It is interesting to know that the majority of coalescence of droplets in our system takes place by coalescing droplets of different, yet adjacent, sizes. The percentage of coalescence of droplets in equal size is generally very small. The identification of such findings opens doors for more detailed mathematical modeling of coalescence mechanism.

Using the coalescence rates predicted by the model, the reconstructed DSDs matched the experimental DSDs closely for all the conditions tested, and this also validated our model. We have also established both specific and generic correlations with both the mean droplet and particle size. In polymerization of acrylamide, the PSDs produced in the OBR were of an essentially Gaussian distribution, and the mean particle sizes ranged from 200 to 800 μm, while still maintaining such a distribution. The level of fines produced in the OBR was found to be much lower than that in a conventional STR. We believe that these advantages would make the OBR an attractive alternative for a number of polymerization reactions.

Acknowledgment

The authors wish to thank the EPSRC for the Industrial Case Award with Ciba Speciality Chemicals.

Notation

C_D = orifice discharge coefficient
$d_{v,0.5}$ = mean particle size, m
d_{32} = Sauter mean diameter, m
d_i^* = geometric mean diameter, μm
D = internal tube diameter, m
D_0 = orifice diameter, m
f = oscillation frequency, s^{-1}
F_i = droplet volume fraction
N_B = number of baffles per unit length, m^{-1}
P/V = power density, $W \cdot m^{-3}$
Re_0 = oscillatory Reynolds number
St = Strouhal number
$x_o f$ = oscillation velocity, $m \cdot s^{-1}$
x_o = oscillation amplitude, m
y = number of datasets

Greek letters

α = ratio of the effective baffle orifice area to the tube area
$\beta_{i,j}$ = coalescence rate of droplet in size range (i) with droplet in size range (j)
ϵ = power dissipation per unit mass, $W \cdot kg^{-1}$
η = characteristic parameter
ρ = density of fluid, $kg \cdot m^{-3}$
σ = interfacial tension, $N \cdot m^{-1}$
ν = kinematic viscosity, $m^2 \cdot s^{-1}$
ω = angular oscillation frequency, $Rad \cdot s^{-1}$

Literature Cited

Baird, M. H. I., and S. J. Lane, "Droplet Size and Holdup in a Reciprocating Plate Extraction Column," *Chem. Eng. Sci.*, **28**, 947 (1973).

Baird, M. H. I., and P. Stonestreet, "Energy Dissipation in Oscillatory Flow Within a Baffled Tube," *Trans. Inst. Chem. Eng.*, **73**, 503 (1995).

Boyadzhiev, L., and M. Spassov, "On the Size of Drops in Pulsed and Vibrating Plate Extraction Columns," *Chem. Eng. Sci.*, **37**, 337 (1982).

Brunold, C. R., J. C. B. Hunns, M. R. Mackley, and J. W. Thompson, "Experimental Observations on Flow Patterns and Energy Losses for Oscillatory Flow in Ducts Containing Sharp Edges," *Chem. Eng. Sci.*, **44**, 1227 (1989).

Coulaloglou, C. A., and L. L. Tavlarides, "Drop Size Distributions and Coalescence Frequencies of Liquid-Liquid Dispersions in Flow Vessels," *AIChE J.*, **22**, 289 (1976).

Coulaloglou, C. A., and L. L. Tavlarides, "Description of Interaction Processes in Agitated Liquid-Liquid Dispersions," *Chem. Eng. Sci.*, **32**, 1289 (1977).

Das, P. K., R. Kumar, and D. Ramkrishna, "Coalescence of Drops in Stirred Dispersion: A White Noise Model for Coalescence," *Chem. Eng. Sci.*, **42**, 213 (1987).

Dickens, A. W., M. R. Mackley, and H. R. Williams, "Experimental Residence Time Distribution Measurements for Unsteady Flow in Baffled Tubes," *Chem. Eng. Sci.*, **44**, 1471 (1989).

Hounslow, M. J., "A Discretized Population Balance for Continuous Systems at Steady State," *AIChE J.*, **36**, 106 (1990).

Hounslow, M. J., R. L. Ryall, and V. R. Marshall, "A Discretized Population Balance for Nucleation, Growth and Aggregation," *AIChE J.*, **34**, 1821 (1988).

Hunkeler, D., and D. E. Haimelec, "Mechanism, Kinetics and Modelling of Inverse-microsuspension Polymerization: 2. Copolymerization of Acrylamide with Quaternary Ammonium Cationic Monomers," *Polymer*, **32**, 2626 (1991).

Hunkeler, D., "Synthesis and Characterization of High Molecular Weight Water-Soluble Polymers," *Polymer Int.*, **27**, 23 (1992).

Hunkeler, D. J., and J. Hernandez-Barajas, "Inverse-Emulsion Polymerization," *Polymeric Materials Encyclopedia*, CRC Press, p. 3322 (1996).

Laso, M., L. Steiner, and S. Hartland, "Dynamic Simulation of Liquid-Liquid Agitated Dispersions: I. Derivation of a Simplified Model," *Chem. Eng. Sci.*, **42**, 2429 (1987).

Lin, C. C., and Y. F. Wang, "Suspension Polymerization of Methyl Methacrylate: I. Modeling of Reaction Kinetics," *J. Appl. Poly. Sci.*, **26**, 3909 (1981).

Litster, J. D., D. J. Smit, and M. J. Hounslow, "Adjustable Discretized Population Balance for Growth and Aggregation," *AIChE J.*, **41**, 591 (1995).

Mackley, M. R., and X. Ni, "Mixing and Dispersion in a Baffled Tube for Steady Laminar and Pulsatile Flow," *Chem. Eng. Sci.*, **46**, 3139 (1991).

Mackley, M. R., and X. Ni, "Experimental Fluid Dispersion Measurements in Periodic Baffled Tube Arrays," *Chem. Eng. Sci.*, **48**, 3293 (1993).

Muralidhar, R., and D. Ramkrishna, "Analysis of Droplet Coalescence in Turbulent Liquid-Liquid Dispersions," *Ind. Eng. Chem. Fundam.*, **25**, 554 (1986).

Muralidhar, R., D. Ramkrishna, P. K. Das, and R. Kumar, "Coalescence of Rigid Droplets in a Stirred Dispersion—II. Band-limited Force Fluctuations," *Chem. Eng. Sci.*, **43**, 1559 (1988).

Narsimhan, G., J. P. Gupta, and D. Ramkrishna, "A Model for Transitional Breakage Probability of Droplets in Agitated Lean Liquid-Liquid Dispersions," *Chem. Eng. Sci.*, **34**, 257 (1979).

Ni, X., Y. Zhang, and I. Mustafa, "Correlation of Polymer Particle

Size with Droplet Size in Suspension Polymerisation of Methylmethacrylate in a Batch Oscillatory-Baffled Reactor," *Chem. Eng. Sci.*, **54**, 841 (1999).
Valentas, K. J., and N. R. Amundson, "Breakage and Coalescence in Dispersed Phase Systems," *I&EC Fundam*., **5**, 533 (1966).
Valentas, K. J., O. Bilous, and N. R. Amundson, "Analysis of Breakage in Dispersed Phase Systems," *I&EC Fundam*, **5**, 271 (1966).
Zeitlin, M. A., and L. L. Tavlarides, "Fluid-Fluid Interactions and Hydrodynamics in Agitated Dispersions: A Simulation Model," *Can. J. Chem. Eng.*, **50**, 207 (1972).
Zerfa, M., and B. W. Brooks, "Prediction of Vinyl Chloride Drop Sizes in a Stabilised Liquid-Liquid Agitated Dispersion," *Chem. Eng. Sci.*, **51**, 3223 (1996).

Manuscript received Feb. 28, 2000, and revision received Jan. 3, 2001.